Inorganics **2015**, *3*, 178-193; doi:10.3390/inorganics3020178

OPEN ACCESS

inorganics

ISSN 2304-6740

www.mdpi.com/journal/inorganics

Article

Biomolecules Electrochemical Sensing Properties of a $PMo_{11}V$@N-Doped Few Layer Graphene Nanocomposite

Diana M. Fernandes [1,*], Marta Nunes [1], Ricardo J. Carvalho [1], Revathi Bacsa [2], Israel-Martyr Mbomekalle [3], Philippe Serp [2], Pedro de Oliveira [3] and Cristina Freire [1,*]

[1] REQUIMTE/LAQV, Departamento de Química e Bioquímica, Faculdade de Ciências, Universidade do Porto, 4169-007 Porto, Portugal; E-Mails: marta.cinderel@hotmail.co (M.N.); r1carvalho4@hotmail.com (R.J.C.)

[2] Laboratoire de Chimie de Coordination UPR CNRS 8241, Composante ENSIACET, Université Toulouse, 4 allée Emile Monso, 31030 Toulouse, France; E-Mails: revathibacsa@gmail.com (R.B.); philippe.serp@ensiacet.fr (P.S.)

[3] Laboratoire de Chimie Physique, UMR 8000 CNRS, Université Paris-Sud, 91405 Orsay Cedex, France; E-Mails: israel.mbomekalle@u-psud.fr (I.-M.M.); pedro.almeida-de-oliveira@u-psud.fr (P.O.)

* Authors to whom correspondence should be addressed; E-Mails: diana.fernandes@fc.up.pt (D.M.F.); acfreire@fc.up.pt (C.F.); Tel.: +351−2204020587 (D.M.F.& C.F.); Fax. +351−220402659 (D.M.F.& C.F.).

Academic Editors: Greta Ricarda Patzke and Pierre-Emmanuel Car

Received: 15 April 2015/ Accepted: 12 May 2015/ Published: 20 May 2015

Abstract: A novel hybrid nanocomposite, $PMo_{11}V$@N-doped few layer graphene, was prepared by a one-step protocol through direct immobilization of the tetrabutylammonium salt of a vanadium-substituted phosphomolybdate ($PMo_{11}V$) onto N-doped few layer graphene (N-FLG). The nanocomposite characterization by FTIR and XPS confirmed its successful synthesis. Glassy carbon modified electrodes with $PMo_{11}V$ and $PMo_{11}V$@N-FLG showed cyclic voltammograms consistent with surface-confined redox processes attributed to Mo-centred reductions ($Mo^{VI} \rightarrow Mo^{V}$) and a vanadium reduction ($V^{V} \rightarrow V^{IV}$). Furthermore, $PMo_{11}V$@N-FLG modified electrodes showed good stability and well-resolved redox peaks with high current intensities. The observed enhancement of $PMo_{11}V$ electrochemical properties is a consequence of a strong electronic communication between the POM and the N-doped few layer graphene. Additionally, the electro-catalytic and sensing properties

towards acetaminophen (AC) and theophylline (TP) were evaluated by voltammetric techniques using a glassy carbon electrode modified with $PMo_{11}V$@N-FLG. Under the conditions used, the square wave voltammetric peak current increased linearly with AC concentration in the presence of TP, but showing two linear ranges: 1.2×10^{-6} to 1.2×10^{-4} and 1.2×10^{-4} to 4.8×10^{-4} mol dm^{-3}, with different AC sensitivity values, 0.022 A/mol dm^{-3} and 0.035 A/mol dm^{-3}, respectively (detection limit, DL = 7.5×10^{-7} mol dm^{-3}).

Keywords: phosphomolybdates; N-doped graphene flakes; nanocomposite; electro-catalysis; biomolecules

1. Introduction

Taking advantage of the electroactivity of some drugs and biomolecules, the application of electrochemical sensors for biological analysis has been growing rapidly, mainly due to the simplicity, accuracy, precision, low cost and rapidity of the electrochemical techniques [1]. In order to develop electrochemical sensors with higher selectivity and sensitivity, the chemical modification of electrode surfaces has been a major focus of research. The modified electrodes present lower overpotential values and improved mass transfer kinetics, decreasing the effect of interferences and avoiding surface fouling [2]. Nanostructured materials, in particular, carbon-based nanomaterials such as carbon nanotubes and graphene, have attracted considerable interest in this field, owing to their unique physical, chemical and electrochemical properties. They present low residual current, readily renewable surfaces and wide potential windows, providing an important and feasible platform for electroanalysis [3,4].

Graphene (G), in particular, emerged as a "superstar" material in the last years, being characterized by a two-dimensional (2D), single-layer sheet of sp^2-hybridized carbon atoms that are closely packed into a hexagonal lattice structure [5]. Its properties, such as fast electron transportation, high thermal conductivity, excellent mechanical strength and high surface area, suggest its ability to detect analyte molecules and to promote a fast electron transfer between the electrode and the analyte, which make it a promising electrocatalyst [3,5]. In fact, several reports published show the good sensitivity and electrocatalytic activity of pristine graphene and graphene-based nanocomposites on the electrochemical sensing of biomolecules such as dopamine (DA) [6,7], uric (UA) and ascorbic (AA) acids [8], nucleic acids [9] and glucose [10].

More recently, advances in graphene research showed that the chemical doping with heteroatoms can be an effective strategy to modulate their electronic properties and surface chemistry. Among the several potential dopants, nitrogen is an excellent candidate due to its comparable size with carbon and five valence-electronic structure, which result in strong covalent bonds between the nitrogen and carbon atoms [11]. The resulting material—nitrogen-doped graphene (N-G)—presents higher electrical conductivity, much larger functional surface area, more biocompatibility and more chemically active sites for functionalization than pristine G [12], whereby it has been applied in N-G-based electrochemical sensors with enhanced performances to the detection of DA, AA and UA [13,14], glucose [15], H_2O_2 [16], antibiotics [17] and pesticides [12].

However, the properties of G-type materials may be yet more prized by the incorporation of these materials in nanocomposites, in order to couple their unique properties with interesting properties of other materials [4,10]. In this context, polyoxometalates (POMs), a kind of transition metal oxide nanoclusters [18], can be a good option owing to their rich chemical and structural variety and, mainly, due to their electronic properties. POMs have the ability to undergo fast, reversible and stepwise multi-electron reactions without decomposition, making them promising electro-catalysts [19]. The incorporation of POMs in nanocomposites with different materials has been reported [20,21]. Several POMs@carbon nanotubes (CNTs) composites have been prepared and applied in batteries [22], supercapacitors [23] and for the reduction of chemical species [24], while POM composites with metal nanoparticles, ionic liquids and conducting polymers have been applied for the reduction of H_2O_2, iodate, nitrite [18,25] and bromate [26], as well as in the sensing of small biomolecules (DA and AA) [19,27]. Previously, we also reported the preparation of several POM@MOFs nanocomposites and their application as electro-catalysts towards nitrite and iodate reductions and AA and DA oxidations [28,29].

Acetaminophen (AC), also known as paracetamol, is an analgesic and antipyretic drug widely used for the relief of mild to moderate pain associated with headache, backache, arthritis and postoperative pain. However, overdoses can lead to the accumulation of toxic metabolites, causing severe and sometimes fatal hepatotoxicity and nephrotoxicity [30]. Theophylline (TP) is a methyl-xanthine derivative which exists widely in nature and is one of the most commonly used medications for the treatment of the symptoms of chronic asthma [3]. Several techniques, including spectrophotometry and liquid chromatography (LC), have been applied for the determination of AC in pharmaceutical formulations and biological fluids, but these methods are time-consuming and expensive. Due to the advantages of low cost, fast response, simple instrumentation and high sensitivity, voltammetric methods are therefore a better solution for the determination of AC in the presence of TP.

This work reports on the preparation of a new nanocomposite, $PMo_{11}V$@N-FLG, by the immobilisation of the tetrabutylammonium salt of vanadium-substituted phosphomolybdate $[PMo_{11}VO_{40}]^{-5}$ ($PMo_{11}V$) into nitrogen-doped few-layer graphene (N-FLG). Investigations were focused on the nanocomposite characterization and its electrochemical properties upon immobilization on a GC electrode surface. The electro-catalytic properties towards AC and TP oxidation were evaluated. In addition, detection of AC in the presence of an excess of TP was also determined.

2. Results and Discussion

2.1. Nanocomposite Preparation and Characterization

The tetra-butylammonium salt of $PMo_{11}V$ was prepared according to the literature and characterized by several techniques [31]. The results obtained are in good agreement with the literature. Figure 1 shows the FTIR spectra of N-FLG, TBA-$PMo_{11}V$ and $PMo_{11}V$@N-FLG. The FTIR spectrum of TBA-$PMo_{11}V$ shows the vibration bands due to the C–H stretching vibration, at 2871 and 2960 cm^{-1}, and those due to C–H bending vibration at 1479 and 1374 cm^{-1} which are characteristic of the TBA salt, two bands in the interval 1080–1040 cm^{-1}, assigned to the splitting of the P–O stretching vibration, a band at 945 cm^{-1} assigned to the Mo–O_d vibration and the bands at 872 cm^{-1} and 799 cm^{-1} to the Mo–O_b–Mo and Mo–O_c–Mo stretching modes, respectively [31–33]. The FTIR spectrum of N-FLG (Figures 1 (black)

and S1) presents very weak and poorly resolved vibrational bands: it shows a broad absorption at around 3455 cm^{-1} assigned to the stretching vibrations of the OH groups which may be due to hydroxyl groups and residual adsorbed water, and the vibration band at 1639 cm^{-1} may be due to C=N stretching vibrations [34]. The two bands at 2855 and 2926 cm^{-1} correspond to the aromatic sp^2 C–H stretching vibration. The sharp band at 1383 cm^{-1} is attributed to C–N stretching vibration [35]. The band at 1533 cm^{-1} is assigned to C=C stretching vibrations of the aromatic carbon, and the band at 1119 cm^{-1} can be assigned to stretching vibration of C–O [36,37].

The preparation of the nanocomposite $PMo_{11}V$@N-FLG was carried out by one-step protocol through the direct immobilization of the prepared TBA-$PMo_{11}V$ onto N-FLG. Accordingly, POM immobilization is based in hydrophobic interactions between the alkyl chains of the TBA cation in the sample with the N-FLG surface, which are also hydrophobic: the POM is linked electrostatically to the TBA cations and consequently adsorbed on the N-FLG surface. However, some interactions between Mo and/or V with the N groups present in the N-FLG cannot be excluded.

FTIR spectrum of the nanocomposite confirms the success of the POM immobilization since it exhibits the bands due to N-FLG in the range 1161 to 1631 cm^{-1}, as well as the vibrational bands due to POM in the range 798–1081 cm^{-1} and TBA at 2960, 2871, 1479 and 1374 cm^{-1}.

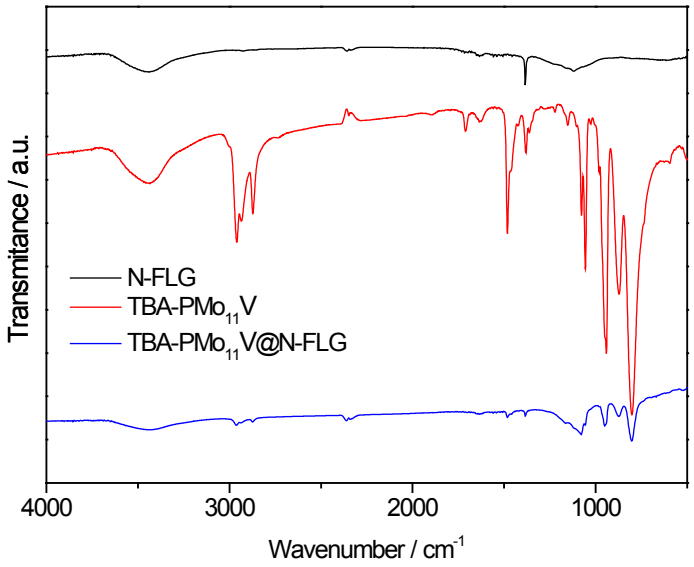

Figure 1. FTIR spectra in the range 4000–500 cm^{-1} for N-FLG (**black**), $PMo_{11}V$ (**red**) and $PMo_{11}V$@N-FLG (**blue**).

The deconvoluted high resolution XPS spectra of N-FLG and $PMo_{11}V$@N-FLG are shown in Figures S2 and S3 as well as the obtained binding energies (Table S1); the surface atomic percentages of each component in both materials are summarized in Table 1. The presence in the nanocomposite of the target elements of each component, N-FLG (C, O, N) and POM (P, Mo, O, N and V) also confirms the successful fabrication of the nanocomposite. The atomic ratios of 1:11 and 1:1 for V:Mo and P:V, respectively, suggest that the POM structure is maintained in the nanocomposite. Furthermore, comparison between the XPS results obtained here with those obtained for the same POM immobilized onto commercial pristine graphene flakes ($PMo_{11}V$@GF) [38] shows that a higher amount of POM was immobilized onto N-FLG which is one advantage for applications in electrochemical sensing.

The C 1s high-resolution spectrum of pristine N-FLG (Figure S2a) was fitted with seven peaks: a main peak at 285.0 eV assigned to the graphitic structure (sp^2), a peak at 286.2 eV attributed to C–C and C–N, a peak at 287.2 eV assigned to C–O, a peak at 288.5 eV related to C=O, a peak at 289.9 eV due to –COO and the peaks at 291.2 and 292.4 eV are attributed to the characteristic shake-up satellite for the π–π^* transition and to its extension, respectively [39,40]. For $PMo_{11}V$@N-FLG, the C 1s high-resolution spectrum (Figure S3a, Table S1) was also fitted with seven peaks: 285.0, 285.8, 286.6, 287.2, 288.2, 289.3 and 291.6 eV with the same assignment as for N-FLG. The slight differences in the peak positions may be due to some structure rearrangements.

The O 1s high resolution spectrum of N-FLG was fitted with two peaks at 531.3 and 533.0 eV ascribed to O=C from ketone, quinone moieties and to O–C from ether and phenol groups, respectively. The $PMo_{11}V$@N-FLG O 1s high resolution spectrum was deconvoluted into three peaks with binding energies at 530.9, 532.1 and 533.6 eV. The last two are assigned as described for N-FLG and the first is ascribed to O–Mo [38].

The N 1s high-resolution spectrum of pristine N-FLG was deconvoluted into four peaks: the peak at 399.1 eV is ascribed to pyridinic-N, the peak at 401.6 eV is attributed to pyrrolic-N, the peak at 404.5 eV is assigned to graphitic N and finally that at 407.3 eV may be due to some oxidized N [39,41,42]. The presence of N on $PMo_{11}V$@N-FLG and its atomic percentage could be assessed, but with low certainty due to the overlap of the N 1s and Mo 3p peaks in the N 1s high resolution spectrum. Nevertheless, the spectrum was fitted taking into consideration the existence of the Mo 3p ($3p_{1/2}$ and $3p_{3/2}$) and N 1s peaks. The area obtained through modulation of Mo 3p is similar to that obtained for Mo 3d, suggesting a correct fitting of peaks taking into consideration the N 1s peaks. The two peaks in the N 1s spectrum at 400.9 and 402.6 eV assigned to pyridinic and pyrrolic-N, respectively. However, two other very low intense peaks could be observed at 404.8 and 406.5 eV, but its low intensity prevent its inclusion in the fitting.

The Mo 3d high resolution spectrum was deconvoluted taking into account the $3d_{5/2}$ and $3d_{3/2}$ doublets caused by spin-orbital coupling. The Mo 3d high resolution spectrum of $PMo_{11}V$@N-FLG was fitted with two couples of peaks with binding energies, respectively, at 231.8 and 234.9 eV assigned to Mo^{5+} and at 233.1 and 236.2 eV assigned to Mo^{6+}. The presence of the Mo^{5+} species suggests that partial photoreduction of POMs occurred when the sample was exposed to the X-ray source or during the nanocomposites preparation.

Table 1. XPS surface atomic percentages for N-FLG and $PMo_{11}V$@N-FLG [a].

Sample	Atomic %					
	C 1s	**O 1s**	**N 1s**	**P 2p**	**V 2p**	**Mo 3d**
N-FLG	91.9	3.8	4.2			
PMo_1V@N-FLG	74.6	16.9	3.1	0.45	0.41	4.4

[a] Determined by the areas of the respective bands in the high-resolution XPS spectra.

2.2. Electrochemical Behaviour

The electroactive surface area of bare GCE, N-FLG/GCE and $PMo_{11}V$@N-FLG/GCE were determined from cyclic voltammograms of 1×10^{-3} mol dm^{-3} $K_3[Fe(CN)_6]$ in KCl 1 mol dm^{-3} (Figure S4) using the Randles-Sevcik equation and assuming that electrode processes are controlled by diffusion:

$$i_{pa} = 2.69 \times 10^5 \, n^{3/2} \, A \, D_r^{1/2} \, R_\infty \, \nu^{1/2} \quad (1)$$

where n is the number of electrons involved in the process (1 in this case), A is the electrode surface area (cm^2), D_r the diffusion coefficient ($cm^2\ s^{-1}$), R the concentration of the species (mol cm^{-3}), ν is the scan rate (V s^{-1}) and i_{pa} the intensity of the anodic peak current (A) [43]. The A values obtained were: 0.0443, 0.0374 and 0.0754 cm^2 for bare GCE, N-FLG/GCE and $PMo_{11}V$@N-FLG/GCE, respectively. These results indicate that the modification of GCE with N-FLG leads to a small decrease of the electroactive area (≈15%) while GCE modification with $PMo_{11}V$@N-FLG/GCE changes dramatically the electroactive area with an increase close to 70%, indicating that the introduction of the $PMo_{11}V$ onto N-FLG provides a more conductive pathway for the electron-transfer of $[Fe(CN)_6]^{3-/4-}$. In addition, the anodic/cathodic peak-to-peak separations (ΔE_p) varies between 0.072 and 0.094 V for GCE, 0.378 and 0.781 V for N-FLG/GCE and 0.076 and 0.086 V for $PMo_{11}V$@N-FLG/GCE for the lowest (0.020 V s^{-1}) and highest (0.50 V s^{-1}) scan rates used.

The electrochemical behaviour of $PMo_{11}V$ and $PMo_{11}V$@N-FLG modified electrodes was studied in pH 2.5 H_2SO_4/Na_2SO_4 buffer solution (Figure 2). In the potential range +0.60 to −0.40 V, the $PMo_{11}V$-modified electrodes revealed five redox processes, denoted as V_1 and Mo_1 to Mo_4, Figure 3a: E_{pcV1} = 0.311 V, E_{pcMo1} = 0.056 V, E_{pcMo2} = −0.058 V, E_{pcMo3} = −0.181 V and E_{pcMo4} = −0.376 V *vs.* Ag/AgCl. Peak V_1 is assigned to a vanadium redox process ($V^V \rightarrow V^{IV}$) and peaks Mo_1 to Mo_4 are attributed to molybdenum redox processes ($Mo^{VI} \rightarrow Mo^V$).

Figure 2b depicts the cyclic voltammograms obtained with a $PMo_{11}V$@N-FLG modified electrode in pH 2.5 H_2SO_4/Na_2SO_4 buffer solution and in the potential range +0.90 to −0.50 V. The nanocomposite also shows five redox processes: E_{pcV1} = 0.317 V, E_{pcMo1} = 0.079 V, E_{pcMo2} = −0.032 V, E_{pcMo3} = −0.227 V and E_{pcMo4} = −0.370 V *vs.* Ag/AgCl, corresponding to one-electron oxidation process of vanadium and four two-electron redox processes assignable to the molybdenum centres. All the peaks are much better resolved and have higher current intensities (≈10 times higher) compared with the POM-modified electrode, suggesting faster electron-transfer kinetics, which is associated with the exceptional electronic properties of N-FLG.

In the experimental timescale employed (scan rates in the range 0.02–0.5 V s^{-1}) both cathodic (E_{pc}) and anodic (E_{pa}) peak potentials varied less than 0.011 V for $PMo_{11}V$ and 0.010 V for $PMo_{11}V$@N-FLG. Figure 3 depicts the plots of log i_p *versus* log v for the Mo_1 and Mo_3 waves of $PMo_{11}V$ and $PMo_{11}V$@N-FLG modified electrodes. Both i_{pc} and i_{pa} are directly proportional to the scan rate for all peaks, with r^2 between 0.998 and 0.991 for $PMo_{11}V$ and 0.998 and 0.992 for $PMo_{11}V$@N-FLG, which indicate surface-confined processes [38]. In addition, the anodic to cathodic peak-to-peak separations (ΔE_p) of all redox couples vary between 0.052 (0.02 V s^{-1}) and 0.019 V (0.5 V s^{-1}) and the ratios i_{pa}/i_{pc} are close to one (0.96 ± 0.05).

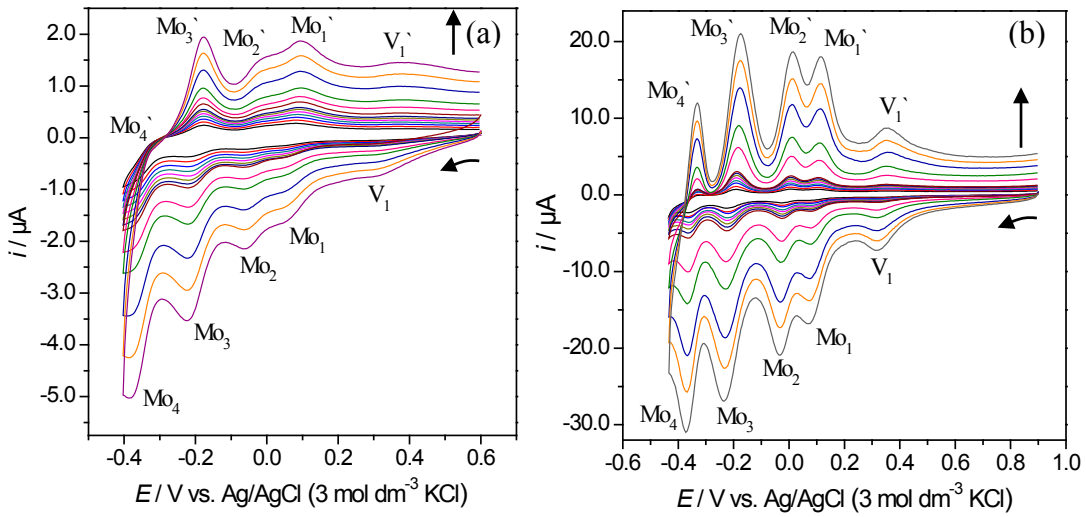

Figure 2. Cyclic voltammograms in pH 2.5 H_2SO_4/Na_2SO_4 buffer solution at different scan rates from 0.02–0.5 V s^{-1} of $PMo_{11}V$ (**a**) and $PMo_{11}V$@N-FLG (**b**).

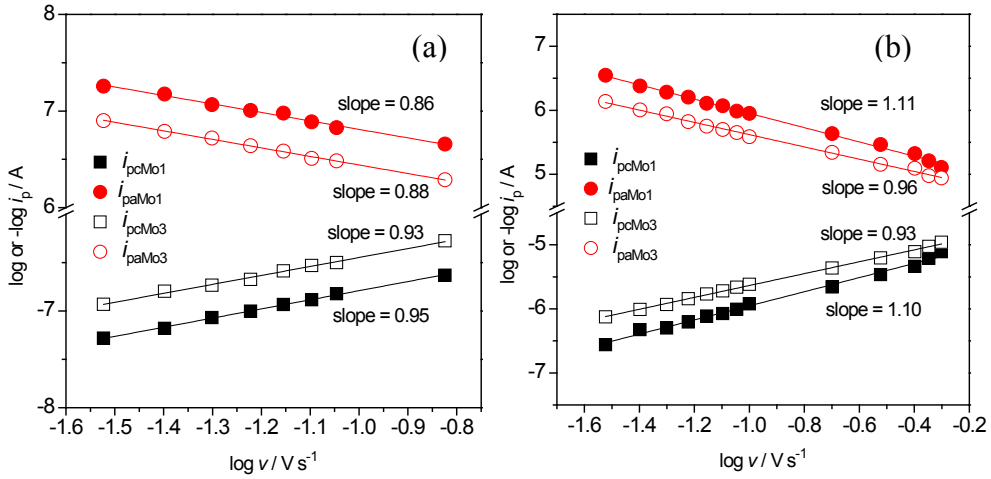

Figure 3. Plots of log i_{pc} and i_{pa} *vs.* log ν of $PMo_{11}V$ (**a**) and $PMo_{11}V$@N-FLG (**b**).

Electrochemical surface coverages of modified electrodes with $PMo_{11}V$ and $PMo_{11}V$@N-FLG were calculated from cyclic voltammetry using the Mo_1 reduction process according to the equation:

$$\Gamma = (4i_pRT)/(n^2F^2vA), \quad (2)$$

where i_p is the peak current (A), n is the number of electrons transferred (2 in this case), v is the scan rate (V s^{-1}), A is the geometric area of the electrode (0.07065 cm^2), R is the gas constant, T is the temperature (298 K) and F is Faraday's constant. Peak currents (Mo_1) were plotted against scan rate (0.02 to 0.5 V s^{-1}) and the value of i_p/v obtained was used to calculate the surface coverage. This led to Γ = 0.006 nmol cm^{-2} for $PMo_{11}V$ and Γ = 0.077 nmol cm^{-2} for $PMo_{11}V$@N-FLG. These results show that electrochemical surface coverage for the nanocomposite modified electrodes is significantly higher (almost 13 times) than that of the POM-modified electrodes. This constitutes an outstanding advantage when developing modified electrodes with carbon nanomaterials for applications in electrocatalysis and electroanalytical determinations. The N-FLG allowed the immobilization of a much larger quantity of

the electroactive $PMo_{11}V$ on the electrode surface due to its high surface area, and simultaneously improved their electrochemical responses.

2.3. Electro-Catalytic Performance of Nanocomposite Modified Electrodes

The electrochemical oxidation of acetaminophen (AC) and theophylline (TP) was initially investigated individually by cyclic voltammetry at the three different electrodes. Figure 4 shows the cyclic voltammograms of 5.0×10^{-4} mol dm^{-3} solutions of AC and TP at a bare GCE and at N-FLG/GCE and $PMo_{11}V$@N-FLG/GCE modified electrodes. With a bare GCE electrode and under the experimental conditions used, AC and TP are irreversibly oxidized at ≈0.762 V and at ≈1.352 V *vs.* Ag/AgCl, respectively.

At a N-FLG modified electrode, the oxidation of TP occurs at almost the same potential as with a bare GCE (1.360 V), and no significant changes are observed in the peak current, whereas for the $PMo_{11}V$@N-FLG modified electrode the peak current increases ≈31% when compared with that obtained with a bare GCE (Figure 4a) and the TP cathodic peak shifts 0.055 V to less positive potentials.

For AC, the modification of a GCE with N-FLG also leads to small differences in the peak currents, but E_{pa} shifts to less positive potentials (E_{pa} = 0.676 V). For $PMo_{11}V$@N-FLG/GCE, the AC oxidation peak is observed at even less positive potentials, *c.a.* E_{pa} = 0.622 V *vs.* Ag/AgCl (E_{pa} cathodic shift of ≈0.140 V when compared to the bare GCE) and the peak current increases by ≈57%, similarly to TP. Additionally, a cathodic peak is observed at E_{pc} ≈ 0.559 V which is attributed to the partial reduction of AC, suggesting that the oxidation of AC in the $PMo_{11}V$@N-FLG modified electrode becomes a quasi-reversible process [36]; the new set of peaks in the potential range 0.45–0.0 V corresponds to the $PMo_{11}V$ redox processes.

These results show that the modification of a GCE with $PMo_{11}V$@N-FLG leads to an improvement in the overall electrochemical performance towards TP and AC oxidations, which is due to the electro-catalytic properties of $PMo_{11}V$.

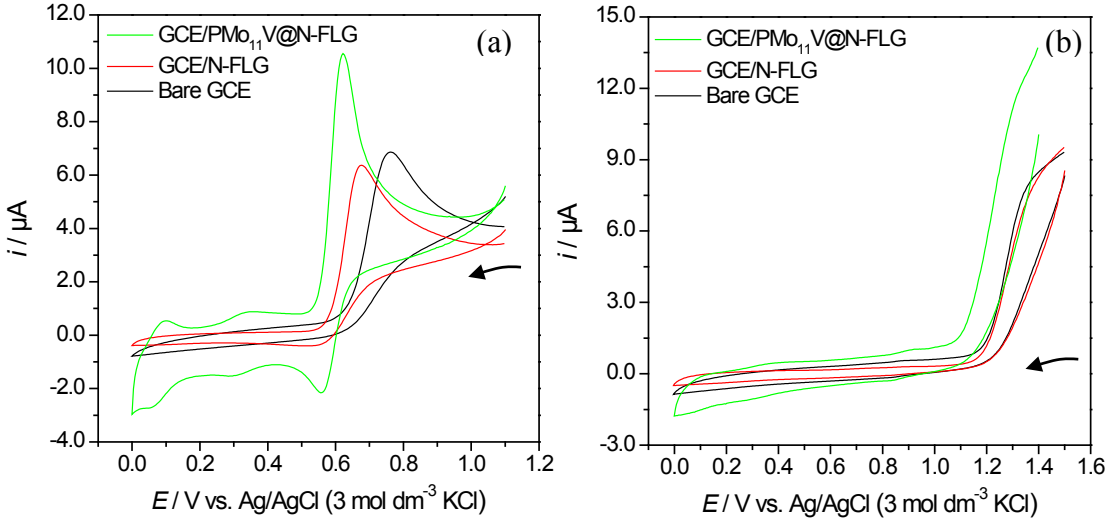

Figure 4. Cyclic voltammograms of 5.0×10^{-4} mol dm^{-3} AC (**a**) and TP (**b**) at a bare GCE, N-FLG/GCE and $PMo_{11}V$@N-FLG/GCE in pH 2.5 H_2SO_4/Na_2SO_4 buffer solution, scan rate 0.050 V s^{-1}.

The electrochemical oxidation of AC and TP was also investigated individually by square wave voltammetry. Figure 5 shows the SWV curves of 5.0×10^{-4} mol dm^{-3} solutions of AC and TP at a bare GCE and at N-FLG/GCE and $PMo_{11}V$@N-FLG/GCE modified electrodes. As observed for cyclic voltammetric results, the immobilization of N-FLG and $PMo_{11}V$@N-FLG on the GCE surface lead to some changes in the square-wave curves of each species when compared to the GCE. At the bare electrode, the oxidation peaks of AC and TP are observed at 0.725 and 1.309 V *vs.* Ag/AgCl.

The modification of a GCE with N-FLG leads to small changes in the oxidation potential of TP, but there is a decrease in peak currents of ≈24%. However, for the oxidation of AC there is an increase of 19% in the peak current and the peak is observed at *c.a.* 0.645 V *vs.* Ag/AgCl (E_{pa} cathodic shift of ≈0.080 V). These changes suggest that N-FLG has itself a strong interaction with the AC species leading to better detection. Still, much more significant results were obtained for GCE modification with the $PMo_{11}V$@N-FLG nanocomposite. For the oxidation of TP there is an increase of the peak currents of 47% and a E_{pa} cathodic shift of 0.045 V, while for the AC oxidation the E_{pa} cathodic shift is 0.126 V and there was an increase of 234% in the peak current, suggesting that this modified electrode is more suitable for the determination of AC rather than TP. These effects are crucial for the application of modified electrodes in electro-catalysis. In a $PMo_{11}V$@N-FLG modified electrode, the high electrical conductivity and large surface area of N-FLG is associated with the unique electro-catalytic properties of $PMo_{11}V$—its ability to accept and release a high number of electrons without decomposition. Consequently, both components contribute to the overall improvement of the electrocatalytic performance. The sensitivity of the $PMo_{11}V$@N-FLG modified electrode towards the oxidation of AC and TP was found to be 0.040 and 0.011 A/mol dm^{-3}, respectively.

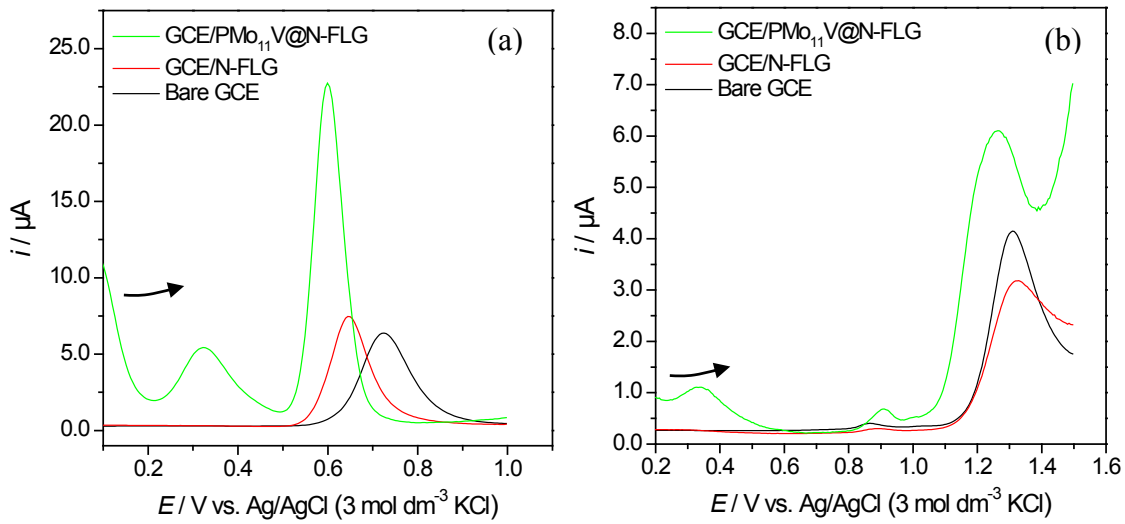

Figure 5. Square wave voltammograms of 5.0×10^{-4} mol dm^{-3} AC (**a**) and TP (**b**) at a bare GCE, N-FLG/GCE and $PMo_{11}V$@N-FLG/GCE in pH 2.5 H_2SO_4/Na_2SO_4 buffer solution, scan rate 0.050 V s^{-1}.

2.4. Determination of AC in the Presence of TP at a $PMo_{11}V$@N-FLG/GCE

Figure 6 shows selected square wave voltammograms recorded for the addition of increasing concentrations of AC. The oxidation peak current of AC increases linearly with the increasing

concentration of AC from 1.2×10^{-6} to 4.8×10^{-4} mol dm^{-3} in the presence of TP: inset in Figure 6. Two different linear regions can be observed: one from 1.2×10^{-6} to 1.2×10^{-4} mol dm^{-3} ($i = 0.022\ c_{AC} + 0.018$, $r^2 = 0.998$), leading to a detection limit 7.5×10^{-7} mol dm^{-3} (detection limit calculated through the equation 3 σ/slope, where σ is the standard deviation of the blank), and a second linear region from 1.2×10^{-4} to 4.8×10^{-4} mol dm^{-3} ($i = 0.035\ c_{AC} - 1.58$, $r^2 = 0.995$). Taking into account that the 'breaking point' in the plot in the inset of Figure 6 corresponds to an AC concentration of 1.2×10^{-4} mol dm^{-3}, which is very similar to the concentration of TP in solution (1.0×10^{-4} mol dm^{-3}), these results may suggest some competition effects between TP and AC: when TP is in larger quantities than AC, a lower AC sensitivity (0.022 A/mol dm^{-3}) is observed when compared to the sensitivity value when AC concentration exceeds that of TP (0.035 A/mol dm^{-3}).

To the best of our knowledge, there are no reports in the literature concerning the use of modified electrodes with a $PMo_{11}V$@N-FLG nanocomposite for the determination of AC in the presence of TP. Furthermore, the obtained detection limit is better than that (8.1×10^{-6} mol dm^{-3}) reported for a similar study at a ferrocene-derivative modified-graphene paste electrode [3].

Finally, the stability and robustness of the $PMo_{11}V$@N-FLG/GCE was evaluated by measuring and comparing the i_{pa} of 0.5 mM AC in a pH 2.5 H_2SO_4/Na_2SO_4 buffer solution at the modified electrode at the begging and at the end of all the experiments (data not shown). No significant change in peak position was observed and the peak current only decreased by 11%, confirming the electrochemical stability of the $PMo_{11}V$@N-FLG modified electrode. This loss might be due to the partial depletion of nanocomposite from the electrode surface due to consecutive use.

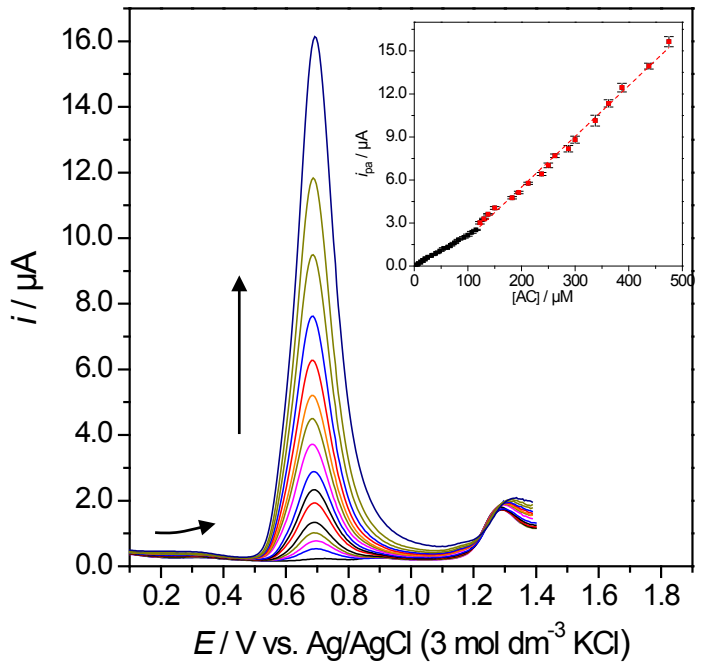

Figure 6. Square-wave voltammetric response at a $PMo_{11}V$@N-FLG/GCE in pH 2.5 buffer solution containing 1.0×10^{-4} mol dm^{-3} TP and different concentrations of AC from 1.2×10^{-6} to 4.8×10^{-4} mol dm^{-3}. Inset: plots of the anodic peak current as a function of the AC concentration.

3. Experimental Section

3.1. Materials and Methods

The N-doped few layer graphene (N-FLG) was prepared by fluidized bed chemical vapor deposition process by the decomposition of a mixture of ethylene and ammonia in the presence of a ternary oxide powder catalyst at 650 °C [44]. The N-FLG powder was recovered after washing the powder in 35% HCl at 25 °C. The tetra-butylammonium salt of the vanadium-phosphomolybdate, $PMo_{11}V$ was prepared according to the literature and characterized by several techniques [31] and the $PMo_{11}V$@N-FLG was prepared using an adapted procedure [38]. Briefly, an acetonitrile solution (2.5 mL) of the compound (20 mg) was added to a toluene dispersion (25 mL) of the N-FLG (20 mg). The resulting yellowish solutions were vigorously stirred at room temperature for 10 min. The solutions were left to rest for 1 h and became colourless (the absence of POM in solution was confirmed by UV-Vis spectroscopy), suggesting a 100% efficiency POM immobilization onto the surfaces of N-FLG, leading to: 1.82 mmol of POM/g nanocomposite. Then, the toluene was removed and the resulting nanocomposite was dried under vacuum at 40 °C.

Theophylline (Fluka), acetaminophen (Sigma-Aldrich, Sintra, Portugal, >99%) and acetonitrile (Romil, Cambridge, UK) were used as received.

The Fourier transform infrared (FTIR) spectra were performed in a Jasco FT/IR-460 Plus spectrophotometer (Jasco, Easton, USA) in the range 400–4000 cm^{-1}, using a resolution of 4 cm^{-1} and 32 scans; the spectra were obtained in KBr pellets (Merck, spectroscopic grade) containing 0.2% weight of $PMo_{11}V$@N-FLG.

The X-ray photoelectron spectroscopy (XPS) measurements were performed at CEMUP (Porto, Portugal), in a VG Scientific ESCALAB 200A spectrometer (VG Scientific, UK) using non-monochromatized Al Kα radiation (1486.6 eV). To correct possible deviations caused by electric charge of the samples, the C 1s band at 285.0 eV was taken as the internal standard. The XPS spectra were deconvoluted with the XPSPEAK 4.1 software (VG Scientific, UK), using non-linear least squares fitting routine after a Shirley-type background subtraction. The surface atomic percentages were calculated from the corresponding peak areas and using the sensitivity factors provided by the manufacturer.

3.2. Electrochemical Studies

An Autolab PGSTAT 30 potentiostat/galvanostat controlled by a GPES software (EcoChimie B.V, Utrecht, The Netherlands) was used for cyclic voltammetry (CV) and square-wave voltammetry (SWV). A conventional three-electrode compartment cell was used. The working electrode was a glassy carbon electrode, GCE, (3 mm diameter, BAS, MF-2012), the auxiliary and reference electrodes were a platinum wire (7.5 cm, BAS, MW-1032) and Ag/AgCl (sat. KCl) (BAS, MF-2052), respectively. The cell was enclosed in a grounded Faraday cage and all studies were carried out at room temperature and kept under an argon flow. A combined glass electrode (Crison) connected to a pH meter Basic 20^{+} (Crison) was used for the pH measurements.

Electrolyte solutions for cyclic voltammetry were prepared using ultra-pure water (resistivity 18.2 MΩ cm at 25 °C, Millipore, Porto, Portugal). The H_2SO_4/Na_2SO_4 buffer solution with pH = 2.5

used for electrochemical studies was prepared by mixing appropriate amounts of a 0.2 mol dm^{-3} H_2SO_4 solution with a 0.5 mol dm^{-3} Na_2SO_4 solution.

The dispersion used to produce the modified electrodes was prepared as follows: a *N*,*N*-dimethylformamide (DMF) dispersion (3 mL) of N-FLG or $PMo_{11}V$@N-FLG (1 mg) was sonicated for 10 min.

Prior to modification, the GCE electrode was conditioned by a polishing/cleaning procedure using diamond pastes of 6, 3 and 1 μm (MetaDi II, Buehler, Düsseldorf, Germany) followed by aluminium oxide of particle size 0.3 μm (Buehler, Düsseldorf, Germany) on a microcloth polishing pad (BAS Bioanalytical Systems Inc., Warsaw, Poland), and then the electrode was rinsed with ultra-pure water and finally sonicated for 5 min in ultra-pure water. Electrode modification consisted in depositing a 3 μL drop of the selected material in dimethylformamide solution onto the surface of the GCE and the solvent was allowed to evaporate for about 30 min at room temperature.

4. Conclusions

The vanadium-substituted phosphomolybdate $PMo_{11}V$ was successfully immobilized on N-doped few layer graphene. X-ray photoelectron spectroscopy revealed that the POM structure was kept in the $PMo_{11}V$@N-FLG nanocomposite. The preparation of modified electrodes with $PMo_{11}V$@N-FLG was easy and quick to perform, leading to reproducible and stable modified electrodes. $PMo_{11}V$@N-FLG/GCE revealed five well defined, surface-confined redox processes that were attributed to four molybdenum centres ($Mo^{VI} \rightarrow Mo^{V}$) and a vanadium centre ($V^{V} \rightarrow V^{IV}$). The $PMo_{11}V$@N-FLG nanocomposite immobilization on a GCE allowed a higher $PMo_{11}V$ surface coverage compared to the direct immobilization of $PMo_{11}V$. This constitutes an outstanding advantage for electrocatalytic and sensing applications: $PMo_{11}V$@N-FLG showed excellent electrocatalytic properties towards AC and TP oxidations and allowed the detection of AC in the presence of an excess of TP.

Acknowledgments

The authors thank Fundação para a Ciência e a Tecnologia (FCT, Portugal) for financial support through projects PEst-C/EQB/LA0006/2013, FCOMP-01-0124-FEDER-037285 and Operation NORTE-07-0124-FEDER-000067–Nanochemistry. DF (SFRH/BPD/74877/2010) and MN (SFRH/BD/79171/2011) also thank FCT for their grants. Thanks are also due to the COST Action CM-1203 PoCheMoN.

Author Contributions

The synthesis of N-FLG was performed by Revathi Bacsa and Philippe Serp and the synthesis of $PMo_{11}V$ and $PMo_{11}V$@N-FLG by Diana M. Fernandes. Marta Nunes contributed to experiments involving the XPS analysis. The electrochemistry experiments were conducted by Diana M. Fernandes and Ricardo J. Carvalho. Cristina Freire, Israel-Martyr Mbomekalle and Pedro de Oliveira helped in the analysis of data and discussion. Cristina Freire and Diana M. Fernandes supervised the research and were responsible for writing of the manuscript.

Conflicts of Interest

The authors declare no conflict of interest.

References

1. Beitollahi, H.; Taher, M.A.; Hosseini, A. Fabrication of a nanostructure-based electrochemical sensor for simultaneous determination of epinephrine and tryptophan. *Measurement* **2014**, *51*, 156–163.
2. Karimi-Maleh, H.; Moazampour, M.; Ahmar, H.; Beitollahi, H.; Ensafi, A.A. A sensitive nanocomposite-based electrochemical sensor for voltammetric simultaneous determination of isoproterenol, acetaminophen and tryptophan. *Measurement* **2014**, *51*, 91–99.
3. Tajik, S.; Taher, M.A.; Beitollahi, H. Application of a new ferrocene-derivative modified-graphene paste electrode for simultaneous determination of isoproterenol, acetaminophen and theophylline. *Sens. Actuators B Chem.* **2014**, *197*, 228–236.
4. Lawal, A.T. Synthesis and utilisation of graphene for fabrication of electrochemical sensors. *Talanta* **2015**, *131*, 424–443.
5. Wu, S.X.; He, Q.Y.; Tan, C.L.; Wang, Y.D.; Zhang, H. Graphene-Based Electrochemical Sensors. *Small* **2013**, *9*, 1160–1172.
6. Kim, Y.R.; Bong, S.; Kang, Y.J.; Yang, Y.; Mahajan, R.K.; Kim, J.S.; Kim, H. Electrochemical detection of dopamine in the presence of ascorbic acid using graphene modified electrodes. *Biosens. Bioelectron.* **2010**, *25*, 2366–2369.
7. Wang, Y.; Li, Y.M.; Tang, L.H.; Lu, J.; Li, J.H. Application of graphene-modified electrode for selective detection of dopamine. *Electrochem. Commun.* **2009**, *11*, 889–892.
8. Ping, J.F.; Wu, J.; Wang, Y.X.; Ying, Y.B. Simultaneous determination of ascorbic acid, dopamine and uric acid using high-performance screen-printed graphene electrode. *Biosens. Bioelectron.* **2012**, *34*, 70–76.
9. Lim, C.X.; Hoh, H.Y.; Ang, P.K.; Loh, K.P. Direct Voltammetric Detection of DNA and pH Sensing on Epitaxial Graphene: An Insight into the Role of Oxygenated Defects. *Anal. Chem.* **2010**, *82*, 7387–7393.
10. Ruiyi, L.; Juanjuan, Z.; Zhouping, W.; Zaijun, L.; Junkang, L.; Zhiguo, G.; Guangli, W. Novel graphene-gold nanohybrid with excellent electrocatalytic performance for the electrochemical detection of glucose. *Sens. Actuators B Chem.* **2015**, *208*, 421–428.
11. Barsan, M.M.; Prathish, K.P.; Sun, X.; Brett, C.M.A. Nitrogen doped graphene and its derivatives as sensors and efficient direct electron transfer platform for enzyme biosensors. *Sens. Actuators B Chem.* **2014**, *203*, 579–587.
12. Dong, X.; Jiang, D.; Liu, Q.; Han, E.; Zhang, X.; Guan, X.; Wang, K.; Qiu, B. Enhanced amperometric sensing for direct detection of nitenpyram via synergistic effect of copper nanoparticles and nitrogen-doped graphene. *J. Electroanal. Chem.* **2014**, *734*, 25–30.
13. Sheng, Z.H.; Zheng, X.Q.; Xu, J.Y.; Bao, W.J.; Wang, F.B.; Xia, X.H. Electrochemical sensor based on nitrogen doped graphene: Simultaneous determination of ascorbic acid, dopamine and uric acid. *Biosens. Bioelectron.* **2012**, *34*, 125–131.

14. Li, S.M.; Yang, S.Y.; Wang, Y.S.; Lien, C.H.; Tien, H.W.; Hsiao, S.T.; Liao, W.H.; Tsai, H.P.; Chang, C.L.; Ma, C.C.M.; *et al*. Controllable synthesis of nitrogen-doped graphene and its effect on the simultaneous electrochemical determination of ascorbic acid, dopamine, and uric acid. *Carbon* **2013**, *59*, 418–429.
15. Luo, S.P.; Chen, Y.; Xie, A.J.; Kong, Y.; Wang, B.; Yao, C. Nitrogen Doped Graphene Supported Ag Nanoparticles as Electrocatalysts for Oxidation of Glucose. *ECS Electrochem. Lett.* **2014**, *3*, B20–B22.
16. Tian, Y.; Wang, F.L.; Liu, Y.X.; Pang, F.; Zhang, X. Green synthesis of silver nanoparticles on nitrogen-doped graphene for hydrogen peroxide detection. *Electrochim. Acta* **2014**, *146*, 646–653.
17. Borowiec, J.; Wang, R.; Zhu, L.H.; Zhang, J.D. Synthesis of nitrogen-doped graphene nanosheets decorated with gold nanoparticles as an improved sensor for electrochemical determination of chloramphenicol. *Electrochim. Acta* **2013**, *99*, 138–144.
18. Wang, R.Y.; Jia, D.Z.; Cao, Y.L. Facile synthesis and enhanced electrocatalytic activities of organic-inorganic hybrid ionic liquid polyoxometalate nanomaterials by solid-state chemical reaction. *Electrochim. Acta* **2012**, *72*, 101–107.
19. Zhou, C.L.; Li, S.; Zhu, W.; Pang, H.J.; Ma, H.Y. A sensor of a polyoxometalate and Au-Pd alloy for simultaneously detection of dopamine and ascorbic acid. *Electrochim. Acta* **2013**, *113*, 454–463.
20. Ji, Y.; Huang, L.; Hu, J.; Streb, C.; Song, Y.F. Polyoxometalate-functionalized nanocarbon materials for energy conversion, energy storage and sensor systems. *Energy Environ. Sci.* **2015**, *8*, 776–789.
21. Herrmann, S.; Ritchie, C.; Streb, C. Polyoxometalate—conductive polymer composites for energy conversion, energy storage and nanostructured sensors. *Dalton Trans.* **2015**, *44*, 7092–7104.
22. Kawasaki, N.; Wang, H.; Nakanishi, R.; Hamanaka, S.; Kitaura, R.; Shinohara, H.; Yokoyama, T.; Yoshikawa, H.; Awaga, K. Nanohybridization of Polyoxometalate Clusters and Single-Wall Carbon Nanotubes: Applications in Molecular Cluster Batteries. *Angew. Chem. Int. Ed.* **2011**, *50*, 3471–3474.
23. Cuentas-Gallegos, A.; Martinez-Rosales, R.; Baibarac, M.; Gomez-Romero, P.; Rincon, M.E. Electrochemical supercapacitors based on novel hybrid materials made of carbon nanotubes and polyoxometalates. *Electrochem. Commun.* **2007**, *9*, 2088–2092.
24. Guo, W.H.; Xu, L.; Xu, B.B.; Yang, Y.Y.; Sun, Z.X.; Liu, S.P. A modified composite film electrode of polyoxometalate/carbon nanotubes and its electrocatalytic reduction. *J. Appl. Electrochem.* **2009**, *39*, 647–652.
25. Ma, H.Y.; Gu, Y.; Zhang, Z.J.; Pang, H.J.; Li, S.; Kang, L. Enhanced electrocatalytic activity of a polyoxometalates-based film decorated by gold nanoparticles. *Electrochim. Acta* **2011**, *56*, 7428–7432.
26. Papagianni, G.G.; Stergiou, D.V.; Armatas, G.S.; Kanatzidis, M.G.; Prodromidis, M.I. Synthesis, characterization and performance of polyaniline-polyoxometalates (XM12, X = P, Si and M = Mo, W) composites as electrocatalysts of bromates. *Sens. Actuators B Chem.* **2012**, *173*, 346–353.
27. Zhu, W.; Zhang, W.J.; Li, S.; Ma, H.Y.; Chen, W.; Pang, H.J. Fabrication and electrochemical sensing performance of a composite film containing a phosphovanadomolybdate and cobalt(II) tetrasulfonate phthalocyanine. *Sens. Actuators B Chem.* **2013**, *181*, 773–781.

28. Fernandes, D.M.; Granadeiro, C.M.; de Sousa, P.M.P.; Grazina, R.; Moura, J.J.G.; Silva, P.; Paz, F.A.A.; Cunha-Silva, L.; Balula, S.S.; Freire, C. SiW11Fe@ MIL-101(Cr) Composite: A Novel and Versatile Electrocatalyst. *ChemElectroChem* **2014**, *1*, 1293–1300.
29. Fernandes, D.M.; Barbosa, A.D.S.; Pires, J.; Balula, S.S.; Cunha-Silva, L.; Freire, C. Novel Composite Material Polyoxovanadate@MIL-101(Cr): A Highly Efficient Electrocatalyst for Ascorbic Acid Oxidation. *ACS Appl. Mater. Interfaces* **2013**, *5*, 13382–13390.
30. Wang, S.F.; Xie, F.; Hu,R.F. Carbon-coated nickel magnetic nanoparticles modified electrodes as a sensor for determination of acetaminophen. *Sens. Actuators B Chem.* **2007**, *123*, 495–500.
31. Himeno, S.; Ishio, N. A voltammetric study on the formation of V(V)- and V(IV)-substituted molybdophosphate(V) complexes in aqueous solution. *J. Electroanal. Chem.* **1998**, *451*, 203–209.
32. Gaunt, A.J.; May, I.; Sarsfield, M.J.; Collison, D.; Helliwell, M.; Denniss, I.S. A rare structural characterisation of the phosphomolybdate lacunary anion, $[PMo_{11}O_{39}]^{7-}$. Crystal structures of the Ln(III) complexes, $(NH_4)_{11}$ $[Ln(PMo_{11}O_{39})_2]\cdot 16H_2O$ (Ln = Ce^{III}, Sm^{III}, Dy^{III} or Lu^{III}). *Dalton Trans.* **2003**, doi:10.1039/B301995K.
33. Copping, R.; Gaunt, A.J.; May, I.; Sarsfield, M.J.; Collison, D.; Helliwell, M.; Denniss, I.S.; Apperley, D.C. Trivalent lanthanide lacunary phosphomolybdate complexes: a structural and spectroscopic study across the series $[Ln(PMo_{11}O_{39})_2]^{11-}$. *Dalton Trans.* **2005**, doi:10.1039/B500408J.
34. Olalde, B.; Aizpurua, J.M.; Garcia, A.; Bustero, I.; Obieta, I.; Jurado, M.J. Single-walled carbon nanotubes and multiwalled carbon nanotubes functionalized with poly(L-lactic acid): a comparative study. *J. Phys. Chem. C* **2008**, *112*, 10663–10667.
35. Kong, X.K.; Sun, Z.Y.; Chen, M.; Chen, C.L.; Chen, Q.W. Metal-free catalytic reduction of 4-nitrophenol to 4-aminophenol by N-doped graphene. *Energy Environ. Sci.* **2013**, *6*, 3260–3266.
36. Kumarasinghe, A.R.; Samaranayake, L.; Bondino, F.; Magnano, E.; Kottegoda, N.; Carlino, E.; Ratnayake, U.N.; de Alwis, A.A.P.; Karunaratne, V.; Amaratunga, G.A.J. Self-Assembled Multilayer Graphene Oxide Membrane and Carbon Nanotubes Synthesized Using a Rare Form of Natural Graphite. *J. Phys. Chem. C* **2013**, *117*, 9507–9519.
37. Lee, D.W.; de los Santos, L.; Seo, J.W.; Felix, L.L.; Bustamante, A.; Cole, J.M.; Barnes, C.H.W. The Structure of Graphite Oxide: Investigation of Its Surface Chemical Groups. *J. Phys. Chem. B* **2010**, *114*, 5723–5728.
38. Fernandes, D.M.; Freire, C. Carbon Nanomaterial-Phosphomolybdate Composites for Oxidative Electrocatalysis. *ChemElectroChem* **2015**, *2*, 269–279.
39. Wang, Y.; Shao, Y.Y.; Matson, D.W.; Li, J.H.; Lin, Y.H. Nitrogen-Doped Graphene and Its Application in Electrochemical Biosensing. *ACS Nano* **2010**, *4*, 1790–1798.
40. Lipinska, M.E.; Rebelo, S.L.H.; Pereira, M.F.R.; Gomes, J.; Freire, C.; Figueiredo, J.L. New insights into the functionalization of multi-walled carbon nanotubes with aniline derivatives. *Carbon* **2012**, *50*, 3280–3294.
41. Xu, H.Y.; Xiao, J.J.; Liu, B.H.; Griveau, S.; Bedioui, F. Enhanced electrochemical sensing of thiols based on cobalt phthalocyanine immobilized on nitrogen-doped graphene. *Biosens. Bioelectron.* **2015**, *66*, 438–444.

42. Liang, X.Q.; Zhong, J.; Shi, Y.L.; Guo, J.; Huang, G.L.; Hong, C.H.; Zhao, Y.D. Hydrothermal synthesis of highly nitrogen-doped few-layer graphene via solid-gas reaction. *Mater. Res. Bull.* **2015**, *61*, 252–258.
43. Bard, A.J.; Faulkner, L.R. *Electrochemical Methods, Fundamentals and Applications*; Wiley: New York, NY, USA, 2001.
44. Bacsa, R.R.; Cameán, I.; Ramos, A.; Garcia, A.B.; Tishkova, V.; Bacsa, W.S.; Gallagher, J.R.; Miller, J.T.; Navas, H.; Jourdain, V.; *et al*. Few layer graphene synthesis on transition metal ferrite catalysts. *Carbon* **2015**, *89*, 350–360.